On the performance of label-free biosensors based on vertical one-dimensional photonic crystal resonant cavities

Salvatore Surdo and Giuseppe Barillaro*

Dipartimento di Ingegneria dell'Informazione, Università di Pisa, Via G. Caruso 16, 56122, Pisa, Italy
*g.barillaro@iet.unipi.it

Abstract: In this work three Fabry-Perot (FP) resonant cavities based on vertical silicon/air one-dimensional photonic crystals (1DPhCs) featuring different architectures and fluidic functionalities are designed, and the role of key design parameters on their ideal biosensing performance, i.e. surface sensitivity, limit of detection, range of linearity, is investigated. Numerical calculations of the transmission spectra of the 1DPhC FP resonant cavities using the Transfer Matrix Method (TMM), versus thickness of a biolayer simulating biomolecules (e.g. proteins) adsorbed on the 1DPhC FP cavity surfaces, show that biosensors with surface sensitivity up to 300 pm/nm, limit of detection down to 0.07 nm, and high linearity over the range 0-50 nm of biolayer thickness can be achieved.

OCIS codes: (280.4788) Optical sensing and sensors; (230.5298) Photonic crystals; (120.2230) Fabry-Perot; (130.6010) Sensors; (070.5753) Resonators

References and links

1. F. Vollmer, S. Arnold, D. Braun, I. Teraoka, and A. Libchaber, "Multiplexed DNA Quantification by Spectroscopic Shift of Two Microsphere Cavities," Biophys. J. **85**(3), 1974–1979 (2003).
2. H.-C. Ren, F. Vollmer, S. Arnold, and A. Libchaber, "High-Q microsphere biosensor - analysis for adsorption of rodlike bacteria," Opt. Express **15**(25), 17410–17423 (2007).
3. H. Zhu, I. M. White, J. D. Suter, P. S. Dale, and X. Fan, "Analysis of biomolecule detection with optofluidic ring resonator sensors," Opt. Express **15**(15), 9139–9146 (2007).
4. M. Iqbal, M. A. Gleeson, B. Spaugh, F. Tybor, W. G. Gunn, M. Hochberg, T. Baehr-Jones, R. C. Bailey, and L. C. Gunn, "Label-Free Biosensor Arrays Based on Silicon Ring Resonators and High-Speed Optical Scanning Instrumentation," IEEE J. Sel. Top. Quantum Electron. **16**(3), 654–661 (2010).
5. R. W. Boyd and J. E. Heebner, "Sensitive disk resonator photonic biosensor," Appl. Opt. **40**(31), 5742–5747 (2001).
6. D. K. Armani, T. J. Kippenberg, S. M. Spillane, and K. J. Vahala, "Ultra-high-Q toroid microcavity on a chip," Nature **421**(6926), 925–928 (2003).
7. I. M. White, H. Oveys, X. Fan, T. L. Smith, and J. Zhang, "Integrated multiplexed biosensors based on liquid core optical ring resonators and antiresonant reflecting optical waveguides," Appl. Phys. Lett. **89**(19), 191106 (2006).
8. F. Vollmer and S. Arnold, "Whispering-gallery-mode biosensing: label-free detection down to single molecules," Nat. Methods **5**(7), 591–596 (2008).
9. Y. Zhao, X. Zhao, and Z. Gu, "Photonic Crystals in Bioassays," Adv. Funct. Mater. **20**(18), 2970–2988 (2010).
10. S. Mandal, J. M. Goddard, and D. Erickson, "A multiplexed optofluidic biomolecular sensor for low mass detection," Lab Chip **9**(20), 2924–2932 (2009).
11. Y. Guo, H. Li, K. Reddy, H. S. Shelar, V. R. Nittoor, and X. Fan, "Optofluidic Fabry–Pérot cavity biosensor with integrated flow-through micro-/nanochannels," Appl. Phys. Lett. **98**(4), 041104 (2011).
12. M. R. Lee and P. M. Fauchet, "Two-dimensional silicon photonic crystal based biosensing platform for protein detection," Opt. Express **15**(8), 4530–4535 (2007).
13. D. Dorfner, T. Zabel, T. Hürlimann, N. Hauke, L. Frandsen, U. Rant, G. Abstreiter, and J. Finley, "Photonic crystal nanostructures for optical biosensing applications," Biosens. Bioelectron. **24**(12), 3688–3692 (2009).
14. S. Surdo, S. Merlo, F. Carpignano, L. M. Strambini, C. Trono, A. Giannetti, F. Baldini, and G. Barillaro, "Optofluidic microsystems with integrated vertical one-dimensional photonic crystals for chemical analysis," Lab Chip **12**(21), 4403–4415 (2012).

#231728 - $15.00 USD Received 2 Jan 2015; revised 6 Mar 2015; accepted 18 Mar 2015; published 2 Apr 2015

15. S. Surdo, F. Carpignano, L. M. Strambini, S. Merlo, and G. Barillaro, "Capillarity-driven (self-powered) one-dimensional photonic crystals for refractometry and (bio)sensing applications," RSC Adv. **4**(94), 51935–51941 (2014).
16. X. Fan and I. M. White, "Optofluidic microsystems for chemical and biological analysis," Nat. Photonics **5**(10), 591–597 (2011).
17. M. Renilkumar and P. Nair, "Low-loss optical channel drop filters based on high-contrast Si–air photonic crystals by wet anisotropic etching," Appl. Opt. **50**(25), E59–E64 (2011).
18. A. Lipson and E. M. Yeatman, "A 1-D Photonic Band Gap Tunable Optical Filter in (110) Silicon," J. Microelectromech. Syst. **16**(3), 521–527 (2007).
19. J. M. Masson, R. St-Gelais, A. Poulin, and Y.-A. Peter, "Tunable Fiber Laser Using a MEMS-Based In Plane Fabry-Pèrot Filter," IEEE J. Quantum Electron. **46**(9), 1313–1319 (2010).
20. R. St-Gelais, J. Masson, and Y.-A. Peter, "All-silicon integrated Fabry–Pérot cavity for volume refractive index measurement in microfluidic systems," Appl. Phys. Lett. **94**(24), 243905 (2009).
21. J. Vörös, "The Density and Refractive Index of Adsorbing Protein Layers," Biophys. J. **87**(1), 553–561 (2004).
22. E. Özkumur, J. W. Needham, D. A. Bergstein, R. Gonzalez, M. Cabodi, J. M. Gershoni, B. B. Goldberg, and M. S. Unlü, "Label-free and dynamic detection of biomolecular interactions for high-throughput microarray applications," Proc. Natl. Acad. Sci. U.S.A. **105**(23), 7988–7992 (2008).
23. H. A. Macleod, *Thin-Film Optical Filters Fourth Edition* (CRC Press, 2010) pp. 44, 218.
24. T. Vo-Dinh, *Biomedical Photonics Handbook* (CRC Press LLC, 2003).
25. F. Mazda, *Telecommunications Engineer's Reference Book* (Butterworth-Heinemann Ltd,1993)
26. G. T. Reed, *Silicon Photonics The State of The Art* (John Wiley & Sons Ltd, 2008)
27. A. Lipson and E. M. Yeatman, "Low-loss one-dimensional photonic bandgap filter in (110) silicon," Opt. Lett. **31**(3), 395–397 (2006).
28. R. St-Gelais, A. Poulin, and Y.-A. Peter, "Advances in Modeling, Design, and Fabrication of Deep-Etched Multilayer Resonators," J. Lightwave Technol. **30**(12), 1900–1908 (2012).
29. G. Barillaro, L. M. Strambini, V. Annovazzi-Lodi, and S. Merlo, "Optical Characterization of High-Order 1-D Silicon Photonic Crystals," IEEE J. Sel. Top. Quantum Electron. **15**(5), 1359–1367 (2009).
30. S. Surdo, F. Carpignano, G. Silva, S. Merlo, and G. Barillaro, "An all-silicon optical platform based on linear array of vertical high-aspect-ratio silicon/air photonic crystals," Appl. Phys. Lett. **103**(17), 171103 (2013).
31. J. Hu, X. Sun, A. Agarwal, and L. C. Kimerling, "Design guidelines for optical resonator biochemical sensors," J. Opt. Soc. Am. B **26**(5), 1032 (2009).
32. I. M. White and X. Fan, "On the performance quantification of resonant refractive index sensors," Opt. Express **16**(2), 1020–1028 (2008).
33. M. Csele, *Fundamentals of Light Sources and Lasers* (John Wiley & Sons, 2004) pp. 196.
34. M. D. Fernández-Ramos, L. Cuadros-Rodríguez, E. Arroyo-Guerrero, and L. F. Capitán-Vallvey, "An IUPAC-based approach to estimate the detection limit in co-extraction-based optical sensors for anions with sigmoidal response calibration curves," Anal. Bioanal. Chem. **401**(9), 2881–2889 (2011).

1. Introduction

Recently there has been an increased interest in employing optical resonant cavities for the development of integrated label-free biosensors able to detect target molecules of clinical relevance (e.g. DNA, proteins, etc.) with high-sensitivity and low-limit of detection, without the use of fluorescent labels. A number of label-free optical biosensors based on different resonant cavities has been successfully reported, including microspheres [1,2], microrings [3,4], microdisks [5], microtoroids [6], capillary tubes [7,8], and photonic crystals (PhCs) [9 and references within it].

Photonic crystals obtained by periodic arrangement of air-gaps in high refractive index materials (e.g. either glass or silicon) have been efficiently used for the development of both one- (1D) [10,11] and two-dimensional (2D) [12,13] resonant cavities for biosensing applications. Low-limit of detection and high sensitivity have been experimentally demonstrated for such PhC biosensors, thanks to strong confinement of light in the resonant cavity, which yields very narrow resonant modes both in transmission and reflection, and heavy perturbation of the cavity mode due to biomolecule binding on the resonant cavity surface, respectively. Despite the intense experimental work being carried out on both 1D and 2D PhC resonant cavities, theoretical investigations on their biosensing performance (e.g. sensitivity, limit of detection, linearity) versus design parameters has been overlooked.

Among PhCs, vertical silicon/air 1DPhCs have been demonstrated to be very appealing for biosensing applications in the near- and mid-infrared range, where both silicon and biological matter absorption is negligible [14,15]. They inherently feature independent fluidic

#231728 - $15.00 USD Received 2 Jan 2015; revised 6 Mar 2015; accepted 18 Mar 2015; published 2 Apr 2015

(through the air-gaps) and optical (perpendicularly to the air-gaps) paths that enable the realization of integrated "flow-through" biosensors with higher sensitivity and lower limit of detection with respect to standard "flow-over" approaches, on the one hand, as well as the integration of biosensors together with on-chip microfluidic and optical networks for the realization of miniaturized biosensing platforms, on the other hand [16]. Fabry-Perot (FP) resonant cavities obtained by breaking the periodicity of vertical silicon/air 1DPhCs with a half-wave defect have been also successfully reported for tunable filter fabrication [17–19], though their use for sensing applications has been limited to refractometry [20].

In this letter, three vertical silicon/air 1DPhC FP resonant cavities with different architectures and fluidic functionalities are designed, and the role of key design parameters, i.e. Fabry-Perot cavity order and 1DPhC micromirror reflectivity, on their biosensing performance, i.e. surface sensitivity (*S*), limit of detection (LoD), range of linearity (*L*), is analyzed by numerical simulation. Simulation results indicate that biosensors with performance comparable to those of best state-of-the-art resonant architectures can be fabricated by properly tuning design parameters, with surface sensitivity up to S = 300 pm/nm, limit of detection down to LoD = 0.07 nm, and high linearity L for biolayer thickness in the range 0-50 nm.

2. Device concept

Figures 1(a), 2(a), and 3(a) show the three 1DPhC FP resonant cavities that are the subect of investigation of this work, all of which are designed to feature a resonant cavity mode that appears in the transmission spectrum as a relative sharp peak centered at λ_0 = 1550 nm when the cavity is filled with a reference liquid having refractive index n_{ref} = 1.33 RIU (e.g. buffer saline solution [21,22]).

The resonant cavity in Fig. 1(a) consists of two vertical silicon/air quarter-wave 1DPhC micromirrors (design parameters $d_{Si} = \lambda_0/4n_{Si}$ = 111.35 nm and $d_{Air} = \lambda_0/4$ = 387.5 nm, where d_{Si} and d_{Air} are width of silicon walls and air-gaps, respectively) with a half-wave air-defect of width $d_{cavity} = K\lambda_0/2n_{ref}$ in between, where K is an integer and represents the cavity-order. The two 1DPhC micromirrors are designed to feature a bandgap in the wavelength range centered at λ_0, whereas the half-wave defect is designed to support an optical resonance mode at λ_0. Only the half-wave air-defect has fluidic functionality and can be infiltrated with biological solutions. The resonant cavity in Fig. 2(a) consists of two vertical silicon/air quarter-wave 1DPhC micromirrors (design parameters $d_{Si} = \lambda_0/4n_{Si}$ = 111.35 nm, $d_{Air} = \boldsymbol{\lambda_0/4n_{ref}}$ = 291.35 nm) with a half-wave air-defect of width $d_{cavity} = K\ \lambda_0/2n_{ref}$ in between. Differently from the cavity of Fig. 1(a), in the cavity of Fig. 2(a) both the 1DPhC air-gaps and the half-wave air-defect have fluidic functionality and can be infiltrated with biological solutions. Finally, the resonant cavity of Fig. 3(a) has complementary architecture and fluidic functionality with respect to that of Fig. 1(a). Only the 1DPhC micromirrors have fluidic functionality and can be infiltrated with biological solutions. Design parameters are $d_{Si} = \lambda_0/4n_{Si}$ = 111.35 nm, $d_{Air} = \lambda_0/4n_{ref}$ = 291.35 nm, $d_{cavity} = K\ \lambda_0/2n_{Si}$.

Hereafter, we will refer to the resonant cavities of Fig. 1(a), 2(a), and 3(a) as $(Si/Air)^N Fluid (Si/Air)^N$, $(Si/Fluid)^N Fluid (Si/Fluid)^N$ and $(Si/Fluid)^N Si (Si/Fluid)^N$, respectively, where N denotes the number of elementary high/low refractive index cells composing each one of the 1DPhC micromirrors of the cavity.

3. Modeling approach

Numerical simulations are carried out using the Transfer Matrix Method (TMM) [23], under the hypotheses that the air-gaps with fluidic functionality are filled with the reference liquid and a biolayer with refractive index n_{bio} = 1.465 RIU (e.g. proteins [21,22]) and thickness t ranging from 0 nm to 50 nm uniformly covers their inner silicon surface. This is equivalent to simulate the effect of a biolayer with constant thickness and different surface-coverage filling factors [22]. The maximum value of t is limited to 50 nm, above which the biolayer thickness

#231728 - $15.00 USD Received 2 Jan 2015; revised 6 Mar 2015; accepted 18 Mar 2015; published 2 Apr 2015

is improbable to growth in real applications [21,22]. Optical loss around the working wavelength λ_0 = 1550 nm due to material absorption is neglected, both for silicon, reference liquid, and biological matter [24–26]. Scattering losses due to roughness, value and distribution, of both PhC silicon surfaces [27–29] and biomolecules adsorbed on the PhC surfaces are also neglected with the aim of calculating the ultimate biosensing features of the proposed 1DPhC resonant architectures.

Theoretical transmission spectra of 1DPhC FP resonant cavity versus biolayer thickness are calculated in the range 1540-1570 nm (minimum step 0.01 pm) around the resonance wavelength λ_0 as a function of the cavity-order K (from 1 to 15), as well as of the number of silicon/air cells N (from 2 to 5) of vertical 1DPhC micromirrors. The transmission spectra are obtained by calculating for each wavelength value in the investigated range the complex transmission coefficient T according to the following expression valid for a multilayer structure with M layers [23]:

$$T = E_T / E_I = 1 / P_{11}$$

$$\begin{pmatrix} E_I \\ E_R \end{pmatrix} = \prod_{i=1}^{M} \frac{1}{\tau_{i-1,i}} \begin{bmatrix} e^{j\varphi_{i-1}} & \rho_{i-1,i} \cdot e^{-j\varphi_{i-1}} \\ \rho_{i-1,i} \cdot e^{j\varphi_{i-1}} & e^{-j\varphi_{i-1}} \end{bmatrix} \begin{pmatrix} E_T \\ 0 \end{pmatrix} = \begin{bmatrix} P_{11} & P_{12} \\ P_{21} & P_{22} \end{bmatrix} \begin{pmatrix} E_T \\ 0 \end{pmatrix}$$

where, E_I, E_R and E_T are the amplitudes of incident, reflected and transmitted electric fields, $\rho_{i-1,i}$ and $\tau_{i-1,i}$ are the Fresnel reflection and transmission coefficients of the i^{th} interface, and $\varphi_{i-1} = 2\pi k n_{i-1} d_{i-1}$ is the phase difference due to light traveling trough the i-1th layer, being k the wave number, n_{i-1} the refractive index and d_{i-1} the thickness of the i-1th layer.

Calibration curves are obtained from transmission spectra by plotting the resonance wavelength position versus biolayer thickness, as a function of both K and N. The maximum value of K is set to 15, so as to investigate possible smoothing out of technological constraints by increasing width, and in turn reducing aspect-ratio, of the half-wave defect of the cavity. The maximum value of N is set to 5, above which transmission of optical signals through the 1DPhC micromirrors becomes negligible for real applications [30].

Performance of the three resonant cavities for biosensing applications are compared by taking into account several analytical parameters, as a function of both K and N, namely sensitivity (S), quality factor (Q), limit of detection (LoD), and range of linearity (L). Sensitivity values, by definition the resonance spectral shift versus thickness variation of the adsorbed biolayer $S = \delta\lambda_p/\delta t$, are calculated as the slope of the linear-regression best fitting calibration curve data (when feasible). Quality factor Q, by definition the ratio between resonance wavelength position (λ_p) and full width at half maximum (FWHM) of the transmission spectrum, is calculated from transmission spectra of the resonant cavity without biological matter adsorbed in it (t = 0 nm). Limit of detection LoD, by definition the ratio between resolution R and sensitivity S, is calculated taking R equal to the FWHM value obtained from transmission spectra of the resonant cavity without biological matter adsorbed in it (t = 0 nm) [31, 32]. Range of linearity L is evaluated as the range of biological material thickness within which the calibration curve is linear (R^2>0.99).

4. Results and discussion

4.1 $(Si/Air)^N Fluid (Si/Air)^N$ resonant cavity

The resonant cavity of Fig. 1(a) is representative of 1DPhC FP resonant cavities that have been reported in the literature so far [17, 20]. Figure 1(b) shows transmission spectra of a $(Si/Air)^N Fluid (Si/Air)^N$ resonant cavity with K = 1 and N = 3, for different values of the biolayer thickness t. The resonance cavity mode shifts towards higher wavelengths as t

#231728 - $15.00 USD Received 2 Jan 2015; revised 6 Mar 2015; accepted 18 Mar 2015; published 2 Apr 2015

increases from 0 to 50 nm. Figure 1(c) shows the calibration curve of the resonant cavity

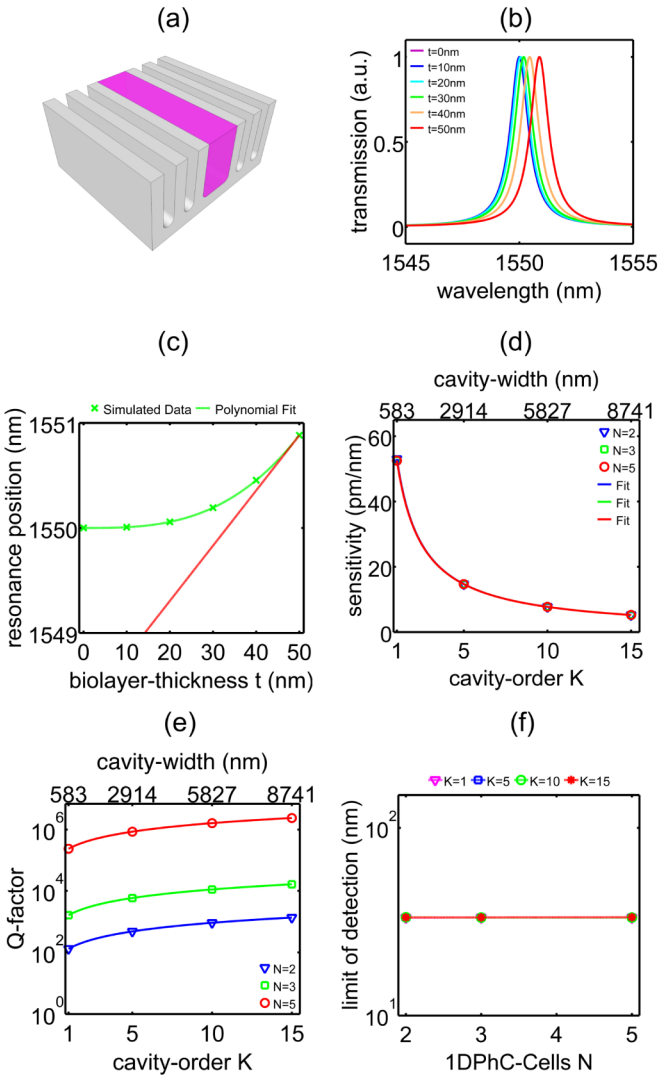

Fig. 1. $(Si/Air)^N Fluid(Si/Air)^N$ resonant cavity: (a) Schematic representation (not to scale) of a 1DPhC-FP-cavity exploiting two vertical silicon/air 1DPhC micromirrors with a half-wave air-defect in between with fluidic functionality. (b) Transmission spectra of the resonant cavity in (a) with K = 1 and N = 3, for biolayer thickness in the range 0-50 nm. (c) Calibration curve of the resonant cavity in (a) with K = 1 and N = 3, for biolayer thickness in the range 0-50 nm. (d) Surface sensitivity of optical biosensor based on the resonant cavity in (a) versus cavity-order K, as a function of the number of cells N of 1DPhC micromirrors. (e) Quality factor Q versus cavity-order K, as a function of the number of cells N of 1DPhC micromirrors. (f) Limit of detection LoD versus number of cells N of 1DPhC micromirrors, as a function of the cavity-order K.

simulated in Fig. 1(b), for which a non-linear shift of the resonant wavelength is apparent within the range of investigated biolayer thicknesses. A similar non-linear behavior of the calibration curve is found for this type of resonant cavity regardless of the value of K and N, thus limiting its practical application in biosensing. Figure 1(d) reports surface sensitivity of this type of resonant cavity versus cavity-order K, for different values of 1DPhC cell-number

#231728 - $15.00 USD Received 2 Jan 2015; revised 6 Mar 2015; accepted 18 Mar 2015; published 2 Apr 2015

N. The sensitivity value is calculated as the maximum slope (see solid line in Fig. 1(c)) of the calibration curve within the investigated range of biolayer thicknesses, for each K and N couple. The surface sensitivity value non-linearly and monotonically decreases as the cavity-order K increases, ranging from about 53 pm/nm (K = 1) to about 5 pm/nm (K = 15) regardless of the value of N. Solid lines in Fig. 1(d) represent best-fitting curves of sensitivity data with the function $S = a/(K + b)$, where a and b are suitable fitting parameters. These results can be explained as follows. For optical biosensors based on resonant structures, the magnitude of the resonance spectral shift is proportional to the surface-to-volume ratio (S/V) of the resonant structure that is subjected to adsorption of biological matter, for a given biolayer thickness [11]. For the resonant cavity of Fig. 1(a) the surface-to-volume ratio value is set by the width of the half-wave defect $S/V = 2/d_{cavity}$, and in turn, by the cavity-order K. The 1DPhC cell-number N does not produce any change to the surface-to-volume ratio value. As the cavity order increases the surface-to-volume ratio decreases, thus reducing the fraction of the resonant mode interacting with the biolayer adsorbed on the surface of the half-wave defect, where the resonant mode itself is mainly confined. This explains the monotonic decrease of the surface sensitivity with K, regardless of the value of N. Figure 1(e) shows quality-factor Q versus cavity-order K as a function of the 1DPhC cell-number N. Both K and N greatly affect the value of Q and, in turn, the theoretical limit of detection of biosensors exploiting the resonant cavity of Fig. 1(a). Typical Q values range from 130 to $2.4\text{x}10^5$ for K = 1 and N variable from 2 to 5, respectively, and from $2.4\text{x}10^5$ to $2.4\text{x}10^6$ for N = 5 and K variable from 1 to 15, respectively. The increase of Q with N can be explained by taking into account the enhancement of 1DPhC micromirror reflectivity as the number of silicon/air cells is increased [23]. On the other hand, by assuming that 1DPhC micromirror losses (reflectivity<1) mostly dominate the resonant cavity losses, and by reminding the energetic definition of the quality factor Q (i.e. 2π times the number of revolution required for the energy that is stored in the cavity to decay to 1/e (≈37%) of the original value [33]), it can be argued that the Q value increases with the cavity-length, and in turn with the cavity-order K, thanks to the reduction of energy-losses per optical cycle, once N is chosen. Figure 1(f) shows limit of detection LoD versus 1DPhC cell-number N, as a function of cavity-order K. LoD values are calculated as intersection between the two linear functions of maximum and minimum slope in the calibration curve, as suggested for sensors with non-linear calibration curve [34]. LoD value results to be about 33 nm for this cavity, regardless of both K and N values.

Summarizing, the $(Si/Air)^N Fluid (Si/Air)^N$ resonant cavity of Fig. 1(a) allows high quality-factor Q to be achieved (order of 10^5-10^6 for N = 5, regardless of K), but the non-linearity of its calibration curve over the investigated range of biolayer thickness (0-50 nm) as well as the consequent high LoD value (about 33 nm, regardless of K and N) significantly limit the exploitation of this cavity for biosensing purposes.

4.2 $(Si/Fluid)^N Fluid (Si/Fluid)^N$ resonant cavity

The resonant cavity of Fig. 2(a), for which both the air-gaps of 1DPhC micromirrors and the half-wave air-defect in between have fluidic functionality, allows addressing the main drawbacks of the cavity of Fig. 1(a) by improving linearity of the calibration curve, reducing limit of detection, and increasing surface sensitivity. Figure 2(b) shows transmission spectra of a $(Si/Fluid)^N Fluid (Si/Fluid)^N$ resonant cavity with K = 1 and N = 3, for different values of the biolayer thickness t. The resonance cavity mode shifts towards higher wavelength as the thickness of the adsorbed biolayer increases from 0 to 50 nm. Note that, for a given biolayer thickness, the magnitude of the shift is significantly larger for this cavity than for the cavity of Fig. 1(a). Figure 2(c) shows the calibration curve of the resonant cavity in Fig. 2(b). A linear shift of the resonance wavelength as the thickness of the biological matter adsorbed on both 1DPhC and half-wave defect surfaces increases from 0 to 50 nm is evident. A similar linear behavior of the calibration curve is found for this type of resonant cavity regardless of the

#231728 - $15.00 USD Received 2 Jan 2015; revised 6 Mar 2015; accepted 18 Mar 2015; published 2 Apr 2015

value of K and N. Figure 2(d) reports surface sensitivity of this type of resonant cavity versus cavity-order K, for different values of N. Sensitivity values are calculated as the slope of the linear-regression best-fitting simulated data of the calibration curve (solid line in Fig. 2(d)), for each K and N couple. As for the resonant cavity of Fig. 1(a), the surface sensitivity non-linearly and monotonically decreases with the cavity-order K, ranging from 121 pm/nm (K = 1, N = 2) to 12 pm/nm (K = 15, N = 2). Solid-lines in Fig. 2(d) show best-fitting of sensitivity data with the function $S = a/(K + b)$, where a and b are suitable fitting parameters. The surface sensitivity value slightly depends on the value of N, once K is given (e.g. K = 1, N = 2, S = 121 pm/nm; K = 1, N = 5, S = 137 pm/nm).

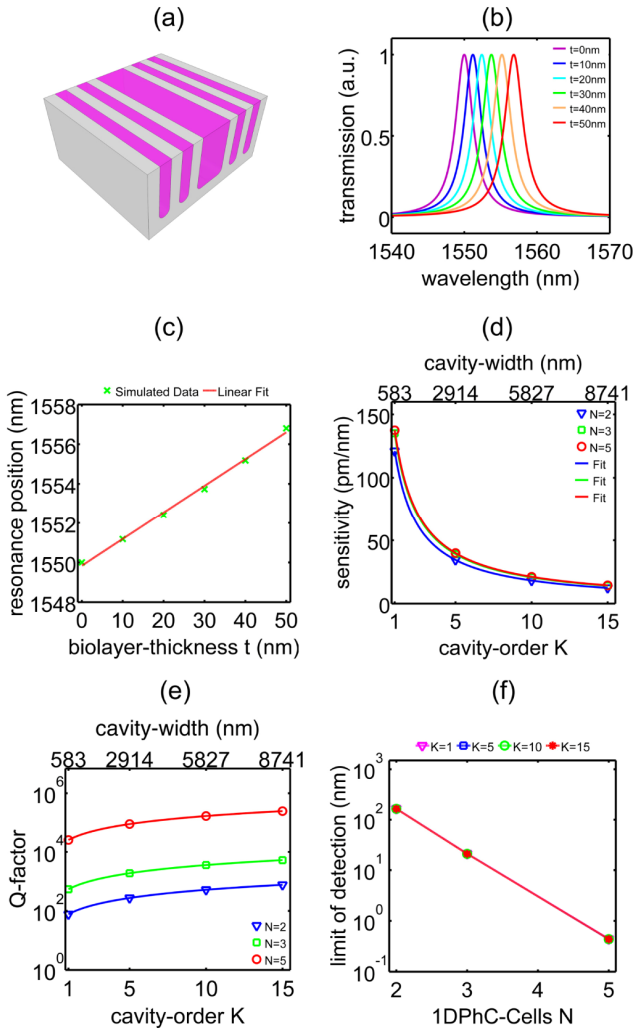

Fig. 2. $(Si/Fluid)^N Fluid(Si/Fluid)^N$ resonant cavity: (a) Schematic representation (not to scale) of a 1DPhC-FP-cavity exploiting two vertical silicon/air 1DPhC micromirrors with a half-wave air-defect in between, all of which with fluidic functionality. (b) Transmission spectra of the resonant cavity in (a) with K = 1 and N = 3, for biolayer thickness in the range 0-50 nm. (c) Calibration curve of the resonant cavity in (a) with K = 1 and N = 3, for biolayer thickness in the range 0-50 nm. (d) Surface sensitivity of optical biosensor based on the resonant cavity in (a) versus cavity-order K, as a function of the number of cells N of 1DPhC micromirrors. (e) Quality factor Q versus cavity-order K, as a function of the number of cells N of 1DPhC micromirrors. (f) Limit of detection LoD versus number of cells N of 1DPhC micromirrors, as a function of the cavity-order K.

#231728 - $15.00 USD Received 2 Jan 2015; revised 6 Mar 2015; accepted 18 Mar 2015; published 2 Apr 2015

Note that, surface sensitivity values of this resonant cavity are more than twice higher than those of the resonant cavity of Fig. 1(a), once K and N are chosen. These results can be explained as follows. By extending fluidic functionality from the half-wave air-defect to the 1DPhC air-gaps, the surface onto which biological matter can be adsorbed/detected also extends (inner surface of the 1DPhC silicon walls), thus enhancing light-matter interaction within the resonant cavity and, in turn, sensitivity with respect to the cavity of Fig. 1(a), once K and N are given. This also explains the slight increase of the surface sensitivity as the number of silicon/air cells N of 1DPhC micromirrors increases. Furthermore, 1DPhC air-gaps width reduces from 387.5 nm, for the cavity of Fig. 1, to 291.35 nm, for the cavity of Fig. 2, thanks to the increased refractive index value of the reference liquid filling the gaps of the 1DPhC with respect to air. This results in an enhancement of the surface-to-volume ratio and, in turn, in the surface sensitivity of biosensors exploiting the resonant cavity of Fig. 2(a).

Figure 2(e) shows quality factor Q versus cavity-order K, as a function of 1DPhC cell-number N. As for the $(Si/Air)^N Fluid(Si/Air)^N$ cavity of Fig. 1(a), both K and N affect the value of Q and, in turn, the theoretical limit of detection of biosensors exploiting this resonant cavity. Typical Q values range from 77 to $2.5x10^4$ for K = 1 and N variable from 2 to 5, respectively, and from $2.5x10^4$ to $2.4x10^5$ for N = 5 and K variable from 1 to 15, respectively. It can be noticed that Q values of this resonant cavity are smaller than those of the resonant cavity of Fig. 1(a), once K and N are chosen. The reduction of Q values can be explained in terms of decreased reflectivity of 1DPhC micromirrors in the cavity of Fig. 2(a) with respect to that of Fig. 1(a) for the same number of cells N, which is related to the reduction in the refractive index contrast of materials composing the 1DPhC micromirrors, silicon/air in Fig. 1(a) and silicon/reference-liquid in Fig. 2(a). Figure 2(f) shows limit of detection LoD versus 1DPhC cell-number N, as a function of cavity-order K. LoD value linearly reduces as N increases, ranging from around 165 nm (N = 2) to 0.438 nm (N = 5), thus improving detection capability of biosensors exploiting such a resonant cavity. Notice that, cavity-order K does not significantly affect LoD values.

Summarizing, the $(Si/Fluid)^N Fluid(Si/Fluid)^N$ resonant cavity of Fig. 2(a) features high sensitivity (up to about 137 pm/nm for K = 1, N = 5) and low limit of detection (down to 0.438 nm for N = 5, regardless of K), with excellent linearity over the whole range 0-50 nm of biolayer thickness investigated.

4.3 $(Si/Fluid)^N Si(Si/Fluid)^N$ resonant cavity

In order to further improve the performance of optical biosensors based on 1DPhC resonant cavities an increase of the surface sensitivity together with a reduction of the limit of detection with respect to the cavity of Fig. 2(a) can be chased up. The 1DPhC resonant cavity of Fig. 3(a) consists of a half-wave silicon-defect between two 1DPhC micromirrors with fluidic functionality. By increasing the refractive index of the half-wave defect from that of the reference liquid (n_{ref} = 1.33 RIU) to that of silicon (n_{Si} = 3.48 RIU) the defect width reduces from 582.71 × K nm to 222.71 × K nm, respectively. This allows reducing the resonant cavity volume of the structure in Fig. 3(a) with respect to that of Fig. 2(a), while maintaining the surface onto which the biological matter can be adsorbed unaltered, once the 1DPhC cell-number N is chosen. The increase in the surface-to-volume ratio is expected to give rise to an increase of the surface sensitivity. Figure 3(b) shows transmission spectra a $(Si/Fluid)^N Si(Si/Fluid)^N$ resonant cavity with K = 1 and N = 3, for different biolayer thicknesses *t*. As for the previous two cavities, the resonance cavity mode shifts towards higher wavelength as the thickness of the adsorbed biolayer increases from 0 to 50 nm. Nonetheless, for a given biolayer thickness, the magnitude of the shift is significantly larger (about two times) for this cavity than for the cavity of Fig. 2(a). Figure 3(c) shows the calibration curve of the resonant cavity in Fig. 3(b). A linear shift of the resonance wavelength as a function of the thickness of biological matter adsorbed on both 1DPhC and half-wave defect silicon surfaces is evident over the whole range of biolayer thicknesses

#231728 - $15.00 USD Received 2 Jan 2015; revised 6 Mar 2015; accepted 18 Mar 2015; published 2 Apr 2015

investigated. A similar linear behavior of the calibration curve is found for this type of resonant cavity regardless of the value of K and N. Figure 3(d) reports surface sensitivity of this type of cavity versus cavity-order K, for different values of N. The sensitivity is calculated as the slope of the linear-regression best-fitting calibration curve data, for each K and N couple. As for the resonant cavities of Fig. 1(a) and 2(a), the surface sensitivity non-linearly and monotonically decreases with the cavity-order K, spanning from 310 pm/nm (K = 1) to 32 pm/nm (K = 15) regardless of N. Notice that, surface sensitivity values are twofold and sixfold those of the cavities in Fig. 2(a) and 1(a), respectively. Solid-lines in Fig. 3(d) show best-fitting of sensitivity data with the function $S = a/(K + b)$, where a and b are suitable fitting parameters.

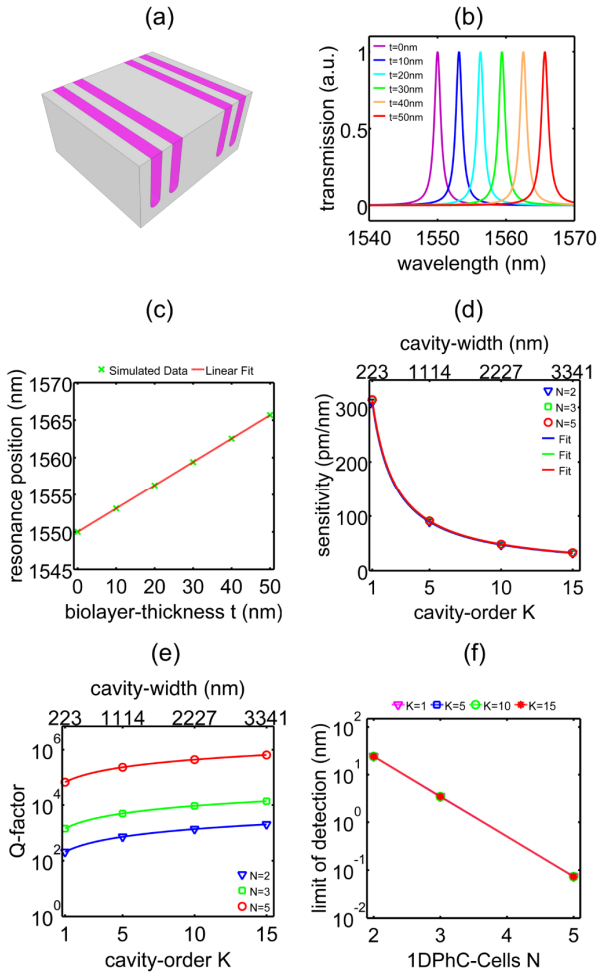

Fig. 3. $(Si/Fluid)^N Si(Si/Fluid)^N$ resonant cavity: (a) Schematic representation (not to scale) of a 1DPhC-FP-cavity exploiting two vertical silicon/air 1DPhC micromirrors featuring fluidic functionality with a half-wave silicon-defect in between. (b) Transmission spectra of the resonant cavity in (a) with K = 1 and N = 3, for biolayer thickness in the range 0-50 nm. (c) Calibration curve of the resonant cavity in (a) with K = 1 and N = 3, for biolayer thickness in the range 0-50 nm. (d) Surface sensitivity of optical biosensor based on the resonant cavity in (a) versus cavity-order K, as a function of the number of cells N of 1DPhC micromirrors. (e) Quality factor Q versus cavity-order K, as a function of the number of cells N of 1DPhC micromirrors. (f) Limit of detection LoD versus number of cells N of 1DPhC micromirrors, as a function of the cavity-order K.

#231728 - $15.00 USD Received 2 Jan 2015; revised 6 Mar 2015; accepted 18 Mar 2015; published 2 Apr 2015

Figure 3(e) shows quality factor Q versus cavity-order K, as a function of 1DPhC cell-number N. The Q value monotonically increases with the number of 1DPhC cells N, as well as with the cavity-order K. Typical Q values range from 205.7 to $6.7x10^4$ for K = 1 and N variable from 2 to 5, respectively, and from $6.7x10^4$ to $6.7x10^5$ for N = 5 and K variable from 1 to 15, respectively. Notice that, once K and N are given, Q values are higher for this cavity than those of the cavity of Fig. 2(a), thanks to the stronger light-confinement in the half-wave silicon-defect with higher refractive index. On the other hand, Q values of this cavity are smaller than those of the cavity of Fig. 1(a), for which 1DPhC micromirrors have higher reflectivity. Figure 3(f) shows limit of detection LoD versus 1DPhC cell-number N, as a function of cavity-order K. LoD linearly reduces as N increases, ranging from about 24 nm (N = 2) to 0.07 nm (N = 5), regardless of cavity-order K. Notice that, LoD values of $(Si/Fluid)^N Si(Si/Fluid)^N$ resonant cavities are about one order of magnitude better that those of $(Si/Fluid)^N Fluid(Si/Fluid)^N$ cavities.

5. Conclusions

In conclusion, the numerical analysis of the ideal performance of biosensors based on three different 1DPhC FP resonant cavities clearly highlights that both architecture and fluidic functionality play a major role on chief sensing parameters, such as surface sensitivity, limit of detection, quality factor, and range of linearity. In addition, for a chosen architecture with a given fluidic functionality, sensitivity and limit of detection mainly depends on the cavity-order K and on the number of 1DPhC cells N, respectively.

On the one hand, $(Si/Air)^N Fluid(Si/Air)^N$ resonant cavities composed of two 1DPhC micromirrors without fluidic functionality with a half-wave silicon-defect in between with fluidic functionality, which have been used in the literature for filtering and sensing applications, seem to have significant limitation for biosensing applications, especially in terms of range of linearity and limit of detection.

On the other hand, best biosensing performance, in terms of sensitivity, limit of detection, and range of linearity are achieved with $(Si/Fluid)^N Si(Si/Fluid)^N$ resonant cavities composed of two 1DPhC micromirrors featuring fluidic functionality with a half-wave silicon-defect in between (S = 300 pm/nm, LoD = 0.07 nm, L = 0-50 nm). For instance, if we refer to a protein biolayer with thickness of 10 nm adsorbed on the 1DPhC resonant cavity surfaces, these numbers mean that this type of resonant cavity can detect the layer of proteins with a shift of 3 nm of the resonance wavelength, which is more than 40 times above the limit of detection of 0.07 nm. Being by definition LoD = 3σ/S, we can estimate the noise of our biosensor as N = 3σ = 21 pm, which allows to conclude that the signal-to-noise ratio for the detection of a 10-nm-thick layer of proteins is estimated as S/N = 143. Such an ideal performance might be affected, in real-world applications, by roughness value and distribution of both PhC silicon surfaces and adsorbed biomolecules on PhC silicon surfaces. The extent to which ideal features will be affected will depend on both fabrication process (as to PhC roughness) and target biomolecules (as to biolayer roughness) and should be taken into account to compare experimental results and theoretical predictions.

Acknowledgments

This activity has been partially funded by the Italian Minister of University and Research (MIUR) “Futuro in Ricerca” (FIR) programme, under the grant N. RBFR122KL1 (SENS4BIO) and by the European Union’s Horizon 2020 research and innovation programme, under the Marie Sklodowska-Curie grant agreement N. 643238 (SYNCHRONICS).